

## ASSESSMENT OF A HIGH RESOLUTION CENTERED SCHEME FOR THE SOLUTION OF HYDRODYNAMICAL SEMICONDUCTOR EQUATIONS\*

A. MARCELLO ANILE<sup>†</sup>, NIKOLAOS NIKIFORAKIS<sup>‡</sup>, AND ROSA M. PIDATELLA<sup>†</sup>

**Abstract.** Hydrodynamical models are suitable to describe carrier transport in submicron semiconductor devices. These models have the form of nonlinear systems of hyperbolic conservation laws with source terms, coupled with Poisson's equation. In this article we examine the suitability of a high resolution centered numerical scheme for the solution of the hyperbolic part of these extended models, in one space dimension. Because of the lack of physically significant exact analytical solutions, the method is assessed against a benchmark for the system of compressible, unsteady Euler equations with source terms, which has an exact solution; the latter is shown to be nearly identical to the numerical one. The method is then used to solve the extended hydrodynamical model (EM) based on the maximum entropy closure recently introduced by Anile, Romano, and Russo, simulating a ballistic diode  $n^+ - n - n^+$ , which models a metal oxide semiconductor field effect transistor (MOSFET) channel. Results are presented for the reduced- and full-equation EM formulation at steady state, for an initially discontinuous electron density at the junctions. Transient results show the evolution of highly nonlinear waves emanating from the neighborhood of the junctions.

**Key words.** semiconductors, high resolution schemes, slope limiter centered

**AMS subject classifications.** 65C20, 65M06

**PII.** S1064827599361588

**1. Introduction.** Enhanced functional integration in modern electron devices requires an accurate modeling of energy transport in semiconductors in order to describe high-field phenomena such as hot-electron propagation, impact ionization, and heat generation in the bulk material. Furthermore, when using compound semiconductors for high frequency applications, usually one deals with multivalley band structures and in these cases the transfer of carriers from one valley to the other must also be modeled. The standard drift-diffusion models cannot cope with high-field phenomena because they do not comprise energy as a dynamical variable. Also they do not incorporate dynamical transfer of carriers from one valley to the other and this renders them ill-suited for simulating time dependent high frequency phenomena. Therefore, generalizations of the drift-diffusion equations have been sought which would incorporate energy as a dynamical variable and which also could treat time dependent high frequency phenomena. Because of their mathematical similarity to the equations of compressible fluid flow, these models are called hydrodynamical models. Semiconductor hydrodynamical models are obtained from the infinite hierarchy of moment equations of the semiclassical Boltzmann transport equation (BTE) by a suitable truncation procedure. This requires making suitable assumptions on (i) choosing the appropriate moments, (ii) closing the hierarchy of moment equations by finding appropriate expressions for the  $N + 1$  order moment in terms of the previous

---

\*Received by the editors September 23, 1999; accepted for publication (in revised form) June 15, 2000; published electronically November 17, 2000. This work was partially supported by a CNR grant (96.03855.CT01) and by the European TMR Programme entitled "Asymptotic Methods in Kinetic Theory," contract ERBFMRXCT970157.

<http://www.siam.org/journals/sisc/22-5/36158.html>

<sup>†</sup>Dipartimento di Matematica, Università di Catania, viale A. Doria 6-95125 Catania, Italy (anile@dipmat.unict.it, rosa@dipmat.unict.it).

<sup>‡</sup>Department of Applied Mathematics and Theoretical Physics, University of Cambridge, Silver Street, Cambridge CB3 9EW, UK (n.nikiforakis@damtp.cam.ac.uk).

ones, and (iii) modeling the production terms on the right-hand side of the moment equations which arise from the moments of the collision terms in the BTE.

Various closure assumptions have been made for the semiconductor transport moment systems, leading to various classes of hydrodynamical models, e.g., [12, 9, 19, 18]. However, these various closure assumptions are, at best, only phenomenological and lack a consistent physical and mathematical justification.

Lately a closure assumption based on the maximum entropy principle of extended thermodynamics [28, 24] or, equivalently, the method of exponential closures [21] has been applied, in the parabolic band approximation, to the semiconductor moment equations, leading to a semiconductor hydrodynamical model free from phenomenological assumptions and enjoying important mathematical properties such as hyperbolicity [5, 4, 6, 8].

With this closure the distribution function used to calculate the higher order moments is assumed to be the one which maximizes the entropy under the constraints of the given set of moments. The resulting constitutive equations for various moments have been compared with the results obtained by Monte Carlo (MC) simulations in [7, 29] and are very encouraging in support of the maximum entropy ansatz. In these models the production terms are modeled by means of a fitting of the MC data for both homogeneous and inhomogeneous doped semiconductors.

**1.1. Previous work on steady-state model integrations.** Apart from the usual balance equations for carrier density, momentum, and energy, these extended models (EMs) comprise evolution equations for the heat flux and shear stress. The resulting system is hyperbolic in a suitable domain of the space of variables.

In the stationary case, by neglecting the viscous stresses and linearizing the heat flux equation for small temperature gradients (Maxwellian iteration) one obtains an extension of the Fourier law which includes also a convective term, which we call the Anile and Pennisi (AP) model [5]. When the convective term in the constitutive equation for the heat flow is (incorrectly) neglected, one obtains the model of Blotekjaer [12] and Baccarani and Wordeman [9] (BBW), which is often used in industrial simulation studies. Gardner, Jerome, and Rose [16] and Gardner [17] numerically integrated the BBW model for a benchmark case study (1-dimensional (1D) quasiballistic  $n^+ - n - n^+$  diode). They discretized the system of equations by using either central differences (if the flow is everywhere subsonic) or the second upwind method (for transonic flow). The discretized system is then linearized by using Newton's method with a damping factor. In this way Gardner [17] was able to show evidence for an electron shock wave in the diode. A method similar to Gardner's was used by Anile, Maccora, and Pidatella [3] in order to solve the AP model with viscosity included. Gardner's results were also recovered within their approach. A similar approach has been used by Benvenuti, Coughran, and Pinto [10] in order to solve coupled thermal hydrodynamical models, using a Galerkin-type formulation.

Another approach which has been used in order to find the steady state for the BBW or AP model (in 1D and 2D) is that of using an artificial time method and mixed finite element space discretization. The ensuing time dependent numerical solutions are evolved until steady state is reached [27].

**1.2. Previous work on time dependent calculations.** The above approaches have dealt with the steady-state system of equations. For several practical applications one has to account for dynamic processes like self-heating of the device, coupling with mechanical effects, etc. This requires that at least the time derivatives in the particle and energy balance equations be reinstated. For recent advanced applications, such

as microwave power generation and optoelectronics, the remaining time derivatives in the momentum and energy-flux equations have to be taken into account.

Numerical solutions of various unsteady semiconductor hydrodynamical models have been presented in various articles. The hyperbolic part of the simpler BBW model coincides with the Euler hydrodynamical equations; shock capturing schemes have been adopted for its solution [15], achieving the stationary solutions as the limit of the time dependent one.

Lately Gruzinskis et al. [18] have applied finite difference methods to solve their hydrodynamical formulation which has a phenomenological closure and obtained wave-like solutions.

Blokhin and Iordanovich [11] have presented numerical solutions for the AP model using a flux vector splitting method, marching the algorithm to steady state.

Similar results have been presented in [31], again for the AP equations, using the Nessyahu–Tadmor (NT) scheme [32] for the convective step, which has the advantage over upwind-based schemes that it does not require the knowledge of the characteristic speeds of the system, which are not known analytically in this case. In their paper Romano and Russo [31] recovered the results obtained by Fatemi, Jerome, and Osher [15] in the case of the BBW model. Further work using the NT scheme was carried out by Anile, Romano, and Russo [7] in order to obtain the steady state for the 1D quasiballistic diode by marching in time the unsteady algorithm.

Since there are no known nontrivial analytical solutions of the EMs against which to compare the numerical results, confidence on the numerical results is enhanced by utilizing other unrelated numerical schemes or by solving mathematically similar problems with known solutions from other disciplines. This motivated recent work on kinetic schemes [2] (which gave results identical to those obtained with the NT scheme, although at a higher computational cost) as well as the work presented in this article.

**2. Rationale for the current numerical approach.** Our intention is to ultimately perform accurate multidimensional calculations of the full time dependent EMs equations to simulate the behavior of realistic devices (bipolar junction transistor (BJT), MOSFET, resonant diodes, etc.) in both transient and steady-state regimes. In this context accuracy means being able to capture small scale wave features (e.g., related to Gunn-type oscillations), as well as the bulk behavior. In this article we have considered the case of a 1D quasiballistic  $n^+ - n - n^+$  diode, which is used as a benchmark problem for models of submicron electron devices, since the salient features of its behavior are understood. The modeling of a realistic device of this kind because of the discontinuous doping profile introduces strong gradients in the initial electron density at the junctions. The subsequent evolution of the system gives rise to nonlinear waves, before reaching a steady state. This implies that we must use methods which do not suffer from excess numerical diffusion or spurious oscillations in the vicinity of steep gradients. Also, although there are “source terms,” the conservation properties of the hyperbolic left-hand side must be maintained. These requirements point us to the *high resolution* family of methods (see, for example, the textbooks by Hirsch [22], LeVeque [26], or Toro [33]) and in particular to those who lend themselves to be combined readily with computational techniques like adaptive mesh refinement (AMR) and modern computer architectures (such as massively parallel computers (MPP)). A typical method of this family offers a conservative discretization, low numerical diffusion, and no spurious oscillations near steep gradients.

High resolution *upwind* methods are most suitable for the numerical solution of systems of hyperbolic conservation laws because they introduce characteristic informa-

tion (regarding the local directionality of the flow) in the evaluation of the numerical fluxes. A great number of upwind high resolution schemes use the solution of the Riemann problem to evaluate the intercell fluxes. However, when the solution of the Riemann problem is not known, it is possible to construct *centered* schemes which do not compromise the qualities of the high resolution family, albeit at a small loss of “sharpness” of the solution.

The solution is updated by evaluating a finite volume formula derived by considering the integral form of the conservation laws. In particular, for a 1D system of the form

$$(2.1) \quad \mathbf{U}_t + \mathbf{F}(\mathbf{U})_x = 0,$$

where  $\mathbf{U}$  and  $\mathbf{F}(\mathbf{U})$  are the vectors of the conserved variables and the fluxes, respectively, and the equivalent integral formulation

$$(2.2) \quad \oint [\mathbf{U} dx + \mathbf{F}(\mathbf{U}) dt] = 0,$$

the resulting update formula is (see [34])

$$(2.3) \quad \mathbf{U}_i^{n+1} = \mathbf{U}_i^n + \frac{\Delta t}{\Delta x} [\mathbf{F}_{i-1/2} - \mathbf{F}_{i+1/2}],$$

where  $\mathbf{U}_i^{n+1}$  and  $\mathbf{U}_i^n$  are the solutions at the next and current time-levels,  $n + 1$  and  $n$ , respectively.  $\mathbf{F}_{i-1/2}$ ,  $\mathbf{F}_{i+1/2}$  are the numerical fluxes<sup>1</sup> at the interfaces of the computational cells of the discretized space; see Figure 2.1. For a given cell width,  $\Delta x$ , and timestep,  $\Delta t$ , the values of the numerical fluxes need to be evaluated in formula (2.3) in order to compute the conserved variables at the next time-level.

To this end centered schemes can be constructed using a nonlinear combination of a good second (or higher) order scheme with a first order monotone scheme.

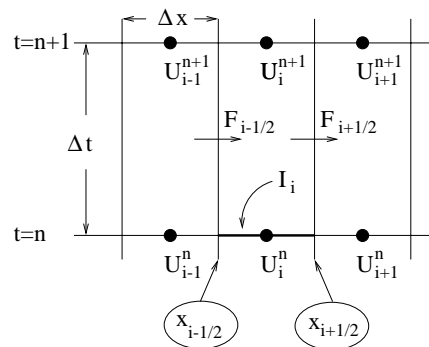


FIG. 2.1. Geometrical representation of the finite volume update formula.

**2.1. The slope limiter centered scheme.** The centered method we use for the calculations presented in this article, namely the slope limiter centered (SLIC) scheme [33], uses a version of the second order MUSCL–Hancock [36] (where MUSCL stands for monotone upstream-centered scheme for conservation laws) and the first-order centered (FORCE) scheme [33]. Since the scheme has been presented elsewhere, we summarize below only its main points, and in particular the ones necessary for our discussion.

<sup>1</sup>The numerical fluxes are approximations to the physical fluxes.

The MUSCL–Hancock approach achieves a second order extension of Godunov’s first order scheme by reconstructing the data as piecewise linear functions in every cell. The left and right cell boundary extrapolated values for cell  $i$

$$\mathbf{U}_i^L = \mathbf{U}_i^n - \frac{1}{2} \Delta_i, \quad \mathbf{U}_i^R = \mathbf{U}_i^n + \frac{1}{2} \Delta_i$$

(where  $\Delta_i$  is a slope vector), are evolved in time by half a timestep as linear combinations of the conserved variables and the fluxes:

$$\begin{aligned} \mathbf{U}_i^{Lnew} &= \mathbf{U}_i^L + \frac{1}{2} \frac{\Delta t}{\Delta x} [\mathbf{F}(\mathbf{U}_i^L) - \mathbf{F}(\mathbf{U}_i^R)], \\ \mathbf{U}_i^{Rnew} &= \mathbf{U}_i^R + \frac{1}{2} \frac{\Delta t}{\Delta x} [\mathbf{F}(\mathbf{U}_i^L) - \mathbf{F}(\mathbf{U}_i^R)]. \end{aligned}$$

However, the intercell fluxes are evaluated using the FORCE scheme, instead of using the solution of the Riemann problem. FORCE is a result of a combination of the Lax–Friedrichs and the Richtmyer schemes (see [33] and references therein). In particular, the flux at the interface of two states  $U_L, U_R$  is

$$(2.4) \quad F_{i+1/2}^{force} \equiv F_{i+1/2}^{force}(U_L, U_R) = 0.5 \left[ F_{i+1/2}^{LF}(U_L, U_R) + F_{i+1/2}^{Ri}(U_L, U_R) \right].$$

In the above expressions, the first order Lax–Friedrichs flux,  $F^{LF}$ , is given by

$$F_{i+1/2}^{LF} \equiv F_{i+1/2}^{LF}(U_L, U_R) = 0.5 [F(U_L) + F(U_R)] + 0.5 \frac{\Delta x}{\Delta t} [U_L + U_R].$$

The second order Richtmyer scheme (which computes a numerical flux by first defining an intermediate state) is

$$U_{i+1/2}^{Ri} \equiv U_{i+1/2}^{Ri}(U_L, U_R) = 0.5(U_L + U_R) + 0.5 \frac{\Delta t}{\Delta x} [F(U_L) - F(U_R)],$$

setting  $F^{Ri} = F(U_{i+1/2}^{Ri})$ .

The resulting scheme is second order accurate in space and time, so to avoid spurious oscillations in the vicinity of steep gradients, the slopes  $\Delta_i$  are replaced by limited slopes  $\bar{\Delta}_i$ , using slope limiter functions. For a detailed exposition of the scheme, the slope limiter functions, and validation problems, see the textbook by Toro [33].

An advantage of the scheme is that every flux component is “limited” independently, using the appropriate conserved variable. This is of paramount importance because normally a single function is used to limit all components; since there is no formal theory on the selection of these functions, this can compromise the performance of the scheme, especially if one flux is continuous at a point in space and time, while another is discontinuous at the same point. Even if a suitable global function is empirically found, this will have to be changed if the equations are altered.

From the above discussion it is evident that once a skeleton algorithm for the scheme is coded, any system of hyperbolic conservation laws can be solved simply by typing the vectors of the conserved variables and the fluxes. For our purposes this is very important because the effects of altering the terms in the conservation laws on the physics of the problem can be readily investigated. For example, in this article we solve the full as well as the reduced EM semiconductor equations; see the following sections.

Also, because the scheme uses a conventional finite volume update formula on a conventional computational mesh, it can be implemented in existing computer program for 2D extensions with or without source terms, as explained in the next section.

**2.2. Fractional steps.** The equations for our problem are of the form

$$(2.5) \quad \frac{\partial \mathbf{U}}{\partial t} + \frac{\partial \mathbf{F}(\mathbf{U})}{\partial x} = \mathbf{S}(\mathbf{U}),$$

coupled with the Poisson equation

$$(2.6) \quad \frac{\partial^2 \Phi}{\partial x^2} = S_1.$$

We adopt the method of fractional steps to evaluate (2.5) and (2.6), where the homogeneous hyperbolic part

$$\frac{\partial \mathbf{U}}{\partial t} + \frac{\partial \mathbf{F}}{\partial \mathbf{U}} = 0$$

is solved using SLIC (with initial and boundary conditions as specified for the complete system), and then we evaluate the remaining ordinary differential equation

$$\frac{\partial \mathbf{U}}{\partial t} = S(\mathbf{U})$$

and the Poisson equation (2.6) using conventional techniques (e.g., Runge–Kutta and tridiagonal matrix solver). Calling  $R$  the relaxation step operator,  $C$  the convection step operator, and  $P$  the Poisson operator, and assuming that the numerical schemes used are at least second order accurate, a Strang splitting [30] which maintains this level of accuracy is

$$\mathbf{U}^{n+1} = R(\Delta t/2)P(\Delta t/2)C(\Delta t)P(\Delta t/2)R(\Delta t/2)\mathbf{U}^n.$$

The accuracy of this splitting and the performance of SLIC for arbitrary source-term driven flow is evaluated using a combustion problem which has an exact solution.

**3. A validation case study.** The scheme has been validated in open literature only for homogeneous systems of equations [33]. Before attempting to implement the semiconductor equations, we validate the scheme against exact solutions of the compressible unsteady Euler equations with source terms using a simplified combustion problem described in some detail by Clarke [13]. It considers flow generated by the action of source terms and is rich in wave structures similar to the ones anticipated in the unsteady evolution of electron flow in semiconductor devices. The governing equations are of the form

$$\mathbf{U}_t + \mathbf{F}(\mathbf{U})_x = \mathbf{S}(\mathbf{U}),$$

where the vectors  $\mathbf{U}$ ,  $\mathbf{F}(\mathbf{U})$ , and  $\mathbf{S}(\mathbf{U})$  are

$$(3.1) \quad \mathbf{U} = \begin{bmatrix} \rho \\ \rho u \\ E \end{bmatrix}, \quad \mathbf{F}(\mathbf{U}) = \begin{bmatrix} \rho u \\ \rho u^2 + p \\ (E + p)u \end{bmatrix}, \quad \mathbf{S}(\mathbf{U}) = \begin{bmatrix} G \\ F \\ H \end{bmatrix}.$$

The right-hand sides  $G$ ,  $F$ , and  $H$  represent general sources of mass, momentum, and energy, while the last two can be written as functions of  $G$ :

$$F = uG, \quad H = (E + p/\rho)G.$$

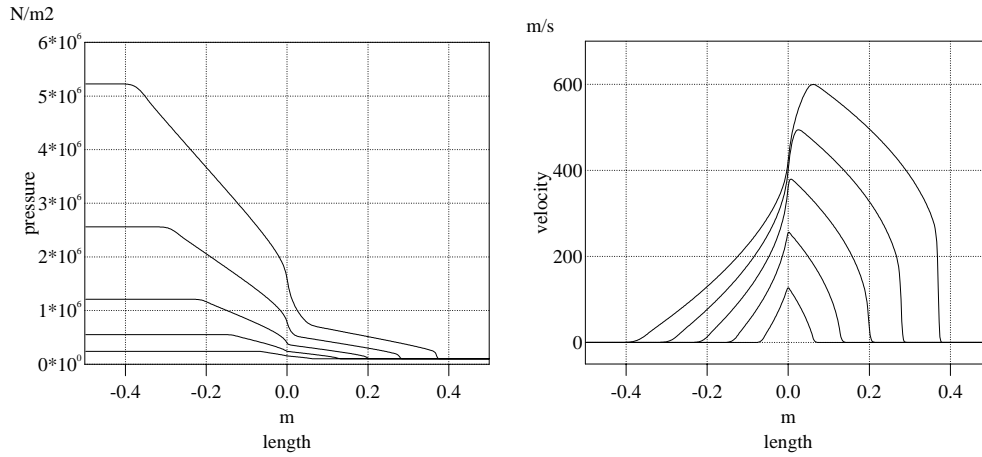


FIG. 3.1. Superimposed numerical (using SLIC) profiles for pressure and velocity at different times, showing the evolution of the flow for the combustion problem formulated in section 3. An expansion wave propagates to the left in a region of increasing pressure, while a compression wave propagates to the right, eventually turning to a shock wave. Sonic flow is observed at the middle of the domain.

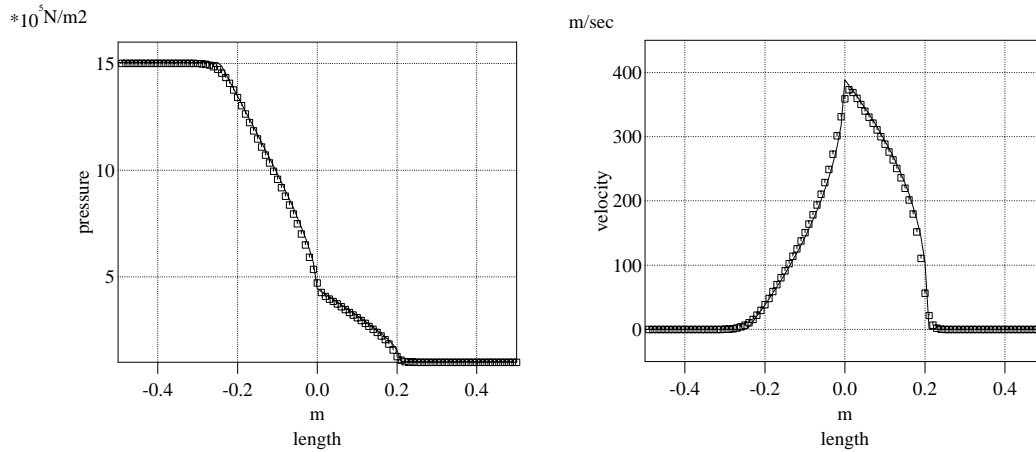


FIG. 3.2. Superimposed exact (line) and numerical (points) solutions using SLIC for the combustion problem formulated in section 3.

An exact solution can be derived if the source term  $G$  is chosen to be such that

$$(aG/\rho) = \bar{G} = \text{const. in } x < 0, \text{ and } \bar{G} = 0 \text{ in } x > 0.$$

Part of the exact solution can be found in the paper by Clarke and Toro [14]. Initially pressure is one atmosphere,  $u = 0$ , and  $a = a_0$ , while the values of the constants are  $a_0 = 330\text{m/sec}$  and  $\bar{G} = 1294301.0\text{m/sec}^2$ .

Profiles of pressure and velocity at different times, mapping the evolution of the flow, are shown in Figure 3.1; these results were obtained using SLIC. The source-driven flow is isentropic up to the time of shock formation ( $t = (4a_0)/((\gamma + 1)\bar{G})$ ) at the head of the wave propagating to the right. Sonic flow conditions appear at  $x = 0$  at  $t = (4a_0)/((3 - \gamma)\bar{G})$ .

Salient features of interest in the context of scheme validation are the rising pressure and the expansion wave in the left (source-filled) part of the domain and the propagating pressure wave in the right part of the domain, which steepens to form a shock wave. An interesting feature of this problem is that the flow “chokes” in the middle of the domain when sonic conditions appear, as indicated by the velocity curves which reach a limit at  $x = 0$  and cusp to the right of the domain.

The accuracy of the method and the correct coupling of the hyperbolic and source-term module is demonstrated in Figure 3.2, which shows superimposed exact (lines) and numerical (points) results at  $t = 0.505 \times 10^{-3}$ ; the two solutions are nearly identical.

**4. Semiconductor equations.** The EMs which we consider here were formulated by Anile, Romano, and Russo [7, 6]. The equations are of the form

$$\mathbf{U}_t + \mathbf{F}(\mathbf{U})_x = \mathbf{S}(\mathbf{U}),$$

where the vectors  $U, F(U)$ , and  $S(U)$  are

$$(4.1) \quad \mathbf{U} = \begin{bmatrix} n \\ nv \\ nv^2 + 3p/m_* \\ \frac{2}{3}nv^2 + \sigma/m_* \\ nv^3 + 5vp/m_* + 2\sigma v/m_* + 2q/m_* \end{bmatrix},$$

$$(4.2) \quad \mathbf{F}(\mathbf{U}) = \begin{bmatrix} nv \\ nv^2 + p/m_* + \sigma/m_* \\ nv^3 + 5vp/m_* + 2\sigma v/m_* + 2q/m_* \\ \frac{2}{3}nv^3 + \frac{4}{3}vp/m_* + \frac{7}{3}v\sigma/m_* + \frac{8}{15}q/m_* \\ nv^4 + 5p^2/n(m_*)^2 + 7\sigma p/n(m_*)^2 + \frac{32}{5}qv/m_* + v^2(8p/m_* + 5\sigma/m_*) + \frac{148}{25}q^2/m_*p \end{bmatrix},$$

$$(4.3) \quad \mathbf{S}(\mathbf{U}) = \begin{bmatrix} 0 \\ -nv/\tau_p - neE/m_* \\ -2(W - W_0)/m_*\tau_W - 2nevE/m_* \\ -1/m_*\tau_\sigma(nv^2 + \sigma/m_*) - 4nevE/3/m_* \\ -1/\tau_q(nv^3 + 5vp/m_* + 2\sigma v/m_* + 2q/m_*) \\ -eE/m_*(3nv^2 + 5p/m_* + 2\sigma/m_*) \end{bmatrix}.$$

Depending on the strength of the electric field, some of the nonlinear terms in the deviation from local thermal equilibrium can be neglected, as well as the anisotropic stresses. Thereby one obtains the following set of equations, which we refer to as the reduced EM. In this case the vectors  $\mathbf{U}, \mathbf{F}(\mathbf{U})$ , and  $\mathbf{S}(\mathbf{U})$  are

$$(4.4) \quad \mathbf{U} = \begin{bmatrix} n \\ nv \\ 3p/m_* \\ 2q/m_* \end{bmatrix},$$

$$(4.5) \quad \mathbf{F}(\mathbf{U}) = \begin{bmatrix} nv \\ p/m_* \\ 2q/m_* \\ 5p^2/n(m_*)^2 \end{bmatrix},$$

$$(4.6) \quad \mathbf{S}(\mathbf{U}) = \begin{bmatrix} 0 \\ -nv/\tau_p - neE/m_* \\ -2(W - W_0)/m_*\tau_w - 2nevE/m_* \\ -1/\tau_q(2q/m_*) - 5eEp/(m_*)^2 \end{bmatrix}.$$

We remark that for the reduced model the interpretation of  $q$  is not that of heat flux but of total energy flux.

In both cases we solve Poisson’s equation:

$$(4.7) \quad \varepsilon \frac{\partial^2 \Phi}{\partial x^2} = -e(N_D - N_A - n), \quad E = -\frac{\partial \Phi}{\partial x}.$$

Here  $n$  is the electron density,  $v$  is the electron velocity,  $p$  is the electron fluid pressure,  $m_*$  is the effective electron mass (taken to be  $0.32 m_e$ ),  $\sigma$  is the anisotropic stress,  $q$  is the heat flux,  $\tau_p$  is the relaxation time for momentum,  $\tau_w$  is the relaxation time for energy,  $\tau_\sigma$  stands for anisotropic stresses,  $\tau_q$  is the relaxation time for the energy flux,  $e$  is the absolute value of the electron charge,  $E$  is the electric field,  $W$  is the energy density,  $W = (1/2)m_*v^2 + (3/2)K_B T$ , and  $W_0$  is the thermal equilibrium energy density.

In both cases the relaxation times are obtained as functions of energy  $W$  from fitting to MC simulation for the same benchmark device (see [29]). The reduced model resembles strongly the so-called energy-transport models obtained from the semiclassical BTE by a Chapman–Enskog-like procedure [1].

**5. A benchmark case study.** As a test problem we consider a ballistic diode  $n^+ - n - n^+$ , which models a MOSFET channel. The diode is made of silicon, and the bulk temperature is supposed to be  $300^\circ\text{K}$ . The  $n^+$  regions are  $0.1\mu\text{m}$  long and the channel length  $L_c$  we consider is  $0.4\mu\text{m}$ . The doping profile is  $N_D^+ = 1. \times 10^{18} \text{ cm}^{-3}$ ,  $N_D = 0.01 \times 10^{18} \text{ cm}^{-3}$ .

For the electron effective mass in the approximation of parabolic band we use  $m_* = 0.32 m_e$ , where  $m_e$  is the electron mass [35]. The silicon dielectric constant is given by  $\epsilon = \epsilon_r \epsilon_0$ , where  $\epsilon_r = 11.7$  is the relative dielectric constant and  $\epsilon_0 = 8.85 \times 10^{-12} \text{ F/m}$   $\mu\text{m}$  is the dielectric constant of vacuum.

The initial electron temperature is the lattice temperature  $T_0 = 300^\circ\text{K}$ , and the charges are at rest. A bias voltage of 1 volt is applied and this determines a charge flux in the semiconductor.

Solutions for the full and the reduced formulation of the equations are shown in this section. In both cases all of the variables are assumed to be initially constant across the computational domain, save for the density of the electrons, which varies discontinuously at the junctions

$$T(x, 0) = 300^\circ\text{K}, \quad v(x, 0) = 0, \quad q(x, 0) = 0, \quad \sigma(x, 0) = 0.$$

The initial density profile is the doping profile, which is an inverted top hat. The total length of the device is  $L = L_c + 0.2\mu\text{m}$ . Transmissive boundary conditions are

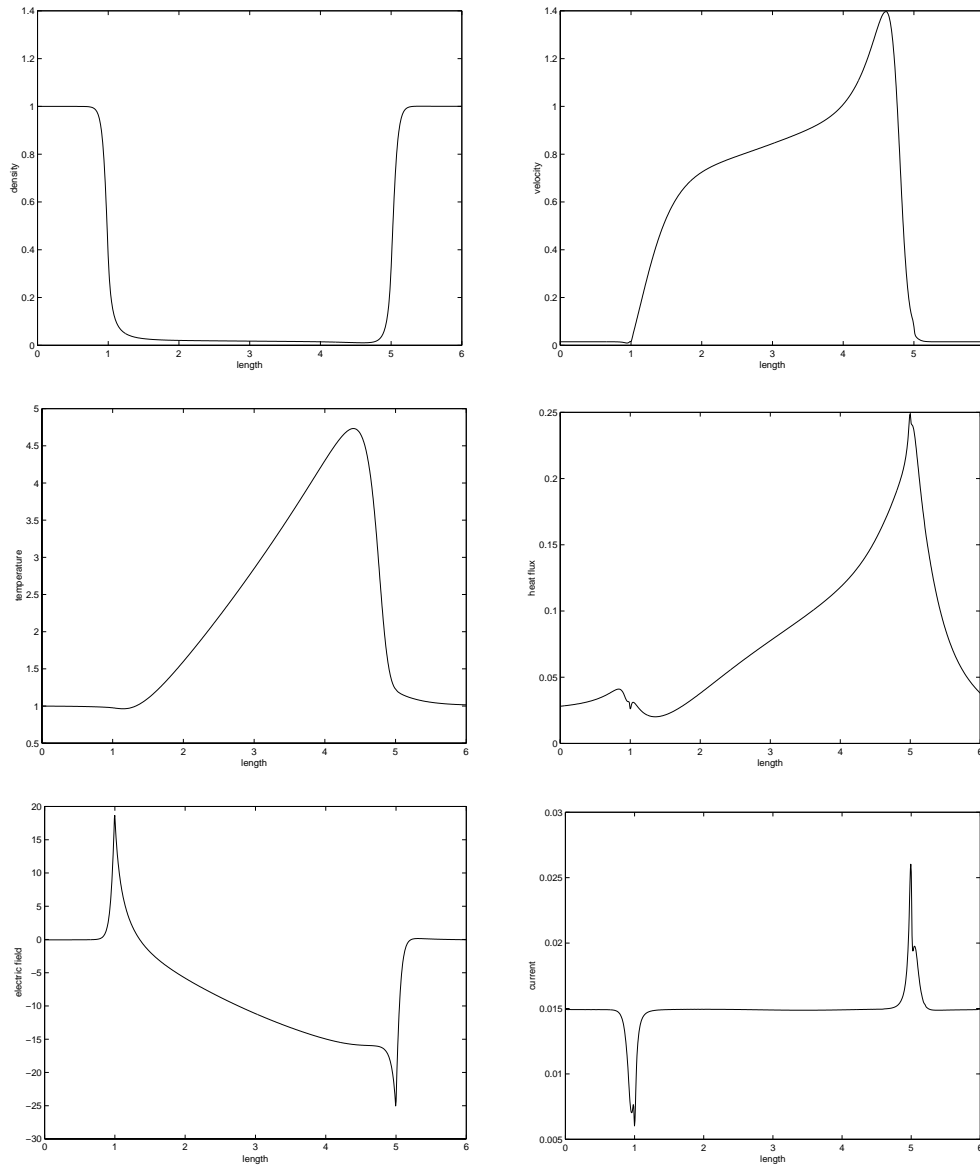


FIG. 5.1. Numerical solutions using SLIC method solving the reduced model  $n^+ - n - n^+$  diode formulation. The initial density distribution was discontinuous at the location of the junctions.

applied at both ends of the computational domain. The boundary conditions for the Poisson's equation are

$$e\Phi(x_{left}) = K_B T \ln(N_D/n_i), \quad e\Phi(x_{right}) = K_B T \ln(N_D/n_i) + eV_{bias},$$

where  $n_i = 1.45 \times 10^{10} \text{cm}^{-3}$  is the intrinsic concentration.

The system is left to evolve, preserving time accuracy, until steady state is reached (results shown at  $t = 5$  picoseconds). The hyperbolic and the source terms are allowed to evolve at different timesteps, which are, however, matched at the end of every iteration. In this way the lower timestep of the source terms does not burden

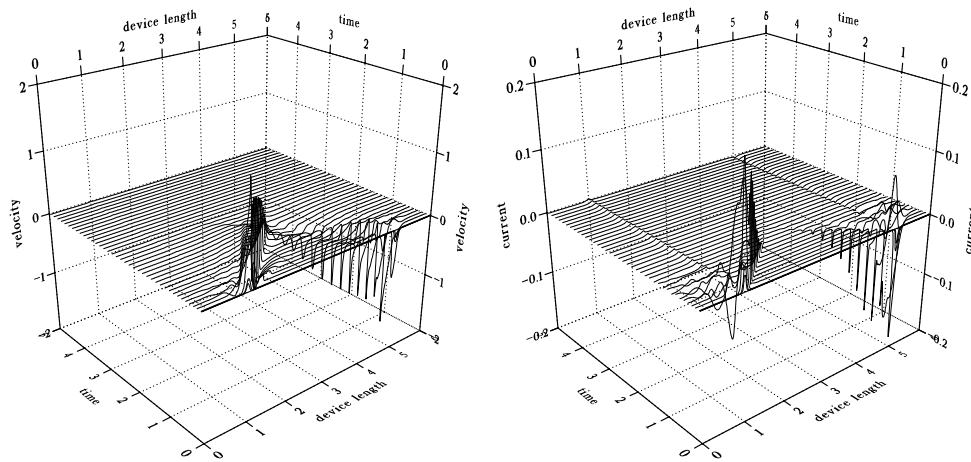


FIG. 5.2. *SLIC method solving the full EM for zero bias (discontinuous initial density). After the initial waves attenuate, velocity reaches a steady-state value of nearly zero (compared with the initial magnitude of the waves), while there is evidence of a small value of current at the location of the junctions.*

the speed of execution of the complete code. It should be noted here that apart from the efficiency issue, marching any method for hyperbolic conservation laws at a timestep smaller than the optimum one, as dictated by the Courant–Friedrichs–Levy (CFL) condition, significantly increases the truncation error of the calculation, which manifests as excessive numerical diffusion.

The thickness of the junctions is of importance to the calculations because, as we will demonstrate in a future communication, it affects some of the salient features in the steady-state profiles of the primitive variables. In any case, the method allows one to vary the junction thickness down to the width of a computational cell, i.e., a genuine discontinuous profile of the initial density, which can match the true physical width of a real device where the doping is obtained by epitaxial growth (and not by ion diffusion). To the best of our knowledge, in all other published results the junctions are smeared over several computational cells and therefore, the resulting simulations apply only to the cases in which the initial profile is obtained by some sort of diffusion.

**5.1. Reduced EM calculations.** The qualitative behavior of the solutions is the same as for the “energy transport” models studied by several researchers [1, 27, 25] under steady-state conditions. The new feature of our approach is that we use a method suitable for hyperbolic systems with source terms, and in this particular case study we evolved the solution as an unsteady problem marched to steady state, preserving time as well as space accuracy. Therefore, our code could be used to investigate the transient behavior of the system from an academic and an engineering point of view. The results of the simulations are shown in Figure 5.1; the initial doping profile is discontinuous at the junctions and the qualitative behavior of the fields is what is expected on physical grounds. Similar results have been obtained where the initial doping is smoothed with a convolution or hyperbolic tangent. In these latter cases the results have been compared with those obtained by a direct solution of the stationary equations using mixed finite elements [37]; the two sets of results agree completely within computer arithmetic. It appears that the current is

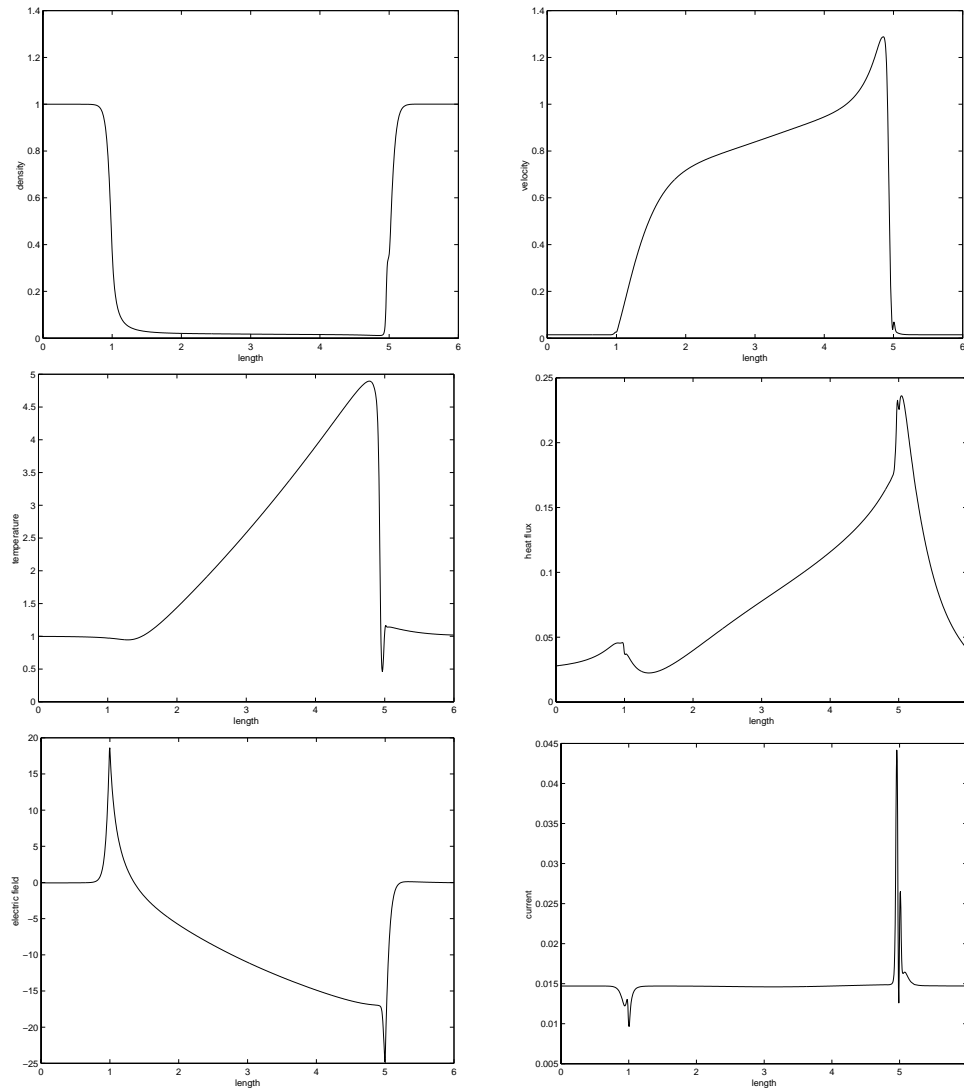


FIG. 5.3. *SLIC method solving the full EM for 1 volt bias (discontinuous initial density); steady-state profiles for various physical variables.*

not exactly constant in the vicinity of the junctions. Previous studies have shown that the magnitude of the error is related to the order of accuracy of the method and, consequently, to the width of the computational cells, i.e., the error can be decreased by using a method of higher order of accuracy. Alternatively, for a given order of accuracy, the error can be decreased by increasing the number of computational cells. The error apparent from Figure 5.1 is of the same order as for similar second order methods and tends to vanish as the number of computational cells increases.

**5.2. Full EM calculations.** The full system of equations was integrated at a zero and a finite-value bias. The former can be used to calculate the junction capacitance and the voltage across the junction. Also, since the velocity and current must go to zero, it also serves as an indication of the accuracy of the numerical model.

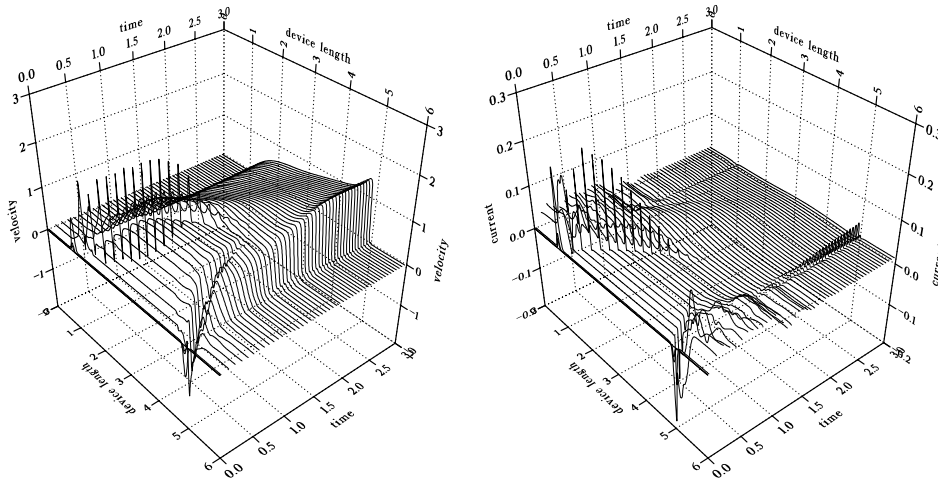


FIG. 5.4. SLIC method solving the full EM for 1 V bias (discontinuous initial density); transient profiles for velocity and current.

The evolution of the field can be seen in Figure 5.2; electrons expand in both directions of the channel, creating electron waves which reach steady state by  $t = 3$  picoseconds. There are no oscillations present in the velocity field, as was reported in the paper by Fatemi, Jerome, and Osher [15]. There is, however, a residual value of current at the location of the junctions, albeit of an order of magnitude smaller than the maximum value reached during this test.

A bias of 1 volt was then applied across the device. Figure 5.3 shows the distribution of the variables at steady state ( $t=5$  picoseconds), while results as a function of time are shown in Figure 5.4. The steady-state plots show no spurious oscillations near steep gradients of the field variables. The small unphysical negative velocity usually observed in the region of the left junction is absent from these calculations. The “bump” usually observed in the vicinity of the right junction is just visible, but not pronounced; initial results suggest that its magnitude and spacial extent is a function of the initial thickness of the junction (the wider the junction, the more pronounced the bump is).

The time-evolution plots show that during the initial stages of the evolution, the strong shock waves (emanating from the locations of the initial density discontinuities) propagate from the junctions towards the middle of the channel. At approximately  $t = 1.5$  they begin to attenuate; the wave propagating from the left adds to the constant increase of the velocity in the middle of the channel, to form the “ramp” of the steady-state velocity profile, while the one from the right contributes to the formation of the pronounced “spike.” The evolution of the latter coincides with the formation of a spike in the current distribution, which persists even after steady state has been reached. If the transient behavior is to be studied in detail, the existence of these strong shock waves necessitates the use of TVD methods.

These results compare favorably to the ones presented in the paper by Anile and Muscato [4], where a direct solution of the steady-state equations is reached using a method similar to Gardner’s [17]. A similar calculation for the transients has been performed by Jerome and Shu [23], albeit for a different model (Baccarani and Wordeman [9]) using an essentially nonoscillatory (ENO) scheme. In both case stud-

ies nonlinear waves arise, but detailed comparison is not meaningful because of the substantial differences in the models.

By comparing the results of the reduced model and of the full model with the same physical and computational parameters, we notice that they differ only slightly (the reduced model shows a higher velocity peak and a lower energy peak), but otherwise the bulk features are essentially the same. Therefore, since the full model presents a more significant computational challenge (in terms of the singularities arising from the nonlinearity and the added computational expense), the reduced model can be used for parametric studies, and once the relevant parameters have been estimated, more detailed simulations can be carried out using the full model.

**6. Conclusions.** A second order scheme for the solution of hyperbolic conservation laws, namely SLIC, has been implemented to solve the extended hydrodynamical semiconductor equations. Other conventional methods have been used to evaluate the source terms and the Poisson equation which is coupled with this system. The scheme is second order accurate in space and time, and it belongs to the high-resolution class of methods. As it is expected from schemes of this class, it is conservative, monotone, and it can resolve discontinuous solutions over very few computational cells.

Our motivation to use this scheme stems from its low computational cost, ease of implementation, and lack of arbitrary, user-adjusted parameters. The current implementation has an automatic selection of the optimum timestep, so that every iteration remains as close as possible to the scheme's stability limit, thus reducing truncation errors and keeping the CPU time as low as possible. Test problems which have an exact solution show that SLIC retains these qualities when used for the integration of a system as complex as the extended hydrodynamical semiconductor equations. Because the scheme does not have user-adjusted parameters and it does not need a special computational stencil, it can be used for multidimensional discretizations on domains of arbitrary geometry and can also be used in conjunction with adaptive mesh refinement software without any implementation complications.

The latest developments in semiconductor technology for ultrafast phenomena in electron devices require new approaches for their numerical simulation. In this article we have implemented a method used in other disciplines which deal with highly nonlinear phenomena and have shown that it is effective in accurately capturing the transient evolution of the electron flow to steady state in a submicron diode.

#### REFERENCES

- [1] N. BEN ABDALLAH AND P. DEGOND, *On a hierarchy of macroscopic models for semiconductors*, J. Math. Phys., 37 (1996), pp. 3306–3333.
- [2] A. M. ANILE, M. JUNK, V. ROMANO, AND G. RUSSO, *Cross-validation of numerical schemes for extended hydrodynamical models of semiconductors*, *M<sup>3</sup>AS*, 10 (2000), pp. 833–861.
- [3] A. M. ANILE, C. MACCORRA, AND R. M. PIDATELLA, *Simulation of  $n^+ - n - n^+$  device by a hydrodynamic model: Subsonic and supersonic flow*, *COMPEL*, 7 (1994), pp. 1–18.
- [4] A. M. ANILE AND O. MUSCATO, *Improved hydrodynamical model for carrier transport in semiconductors*, Phys. Rev. B, 51 (1995), pp. 16728–16740.
- [5] A. M. ANILE AND S. PENNISI, *Thermodynamic derivation of the hydrodynamical model for charge transport in semiconductors*, Phys. Rev. B, 46 (1992), pp. 13186–13193.
- [6] A. M. ANILE, V. ROMANO, AND G. RUSSO, *Hyperbolic Hydrodynamical Model of Carrier Transport in Semiconductors*, *VLSI Design*, 8 (1998), pp. 521–526.
- [7] A. M. ANILE, V. ROMANO, AND G. RUSSO, *Extended hydrodynamical model of carrier transport in semiconductors*, *SIAM J. Appl. Math.*, 61 (2000), pp. 74–101.
- [8] A. M. ANILE AND M. TROVATO, *Nonlinear closures for hydrodynamical semiconductors transport models*, Phys. Lett. A, 230 (1997), pp. 387–395.

- [9] G. BACCARANI AND M. R. WORDEMAN, *An investigation on steady-state velocity overshoot in Silicon*, Solid-state Electronics, 29 (1982), pp. 970–977.
- [10] A. BENVENUTI, W. M. COUGHRAN, JR., AND M. R. PINTO, *A thermally-fully hydrodynamical model for semiconductor devices and applications to III-V HBT simulation*, IEEE Trans. Electron. Devices, 44 (1997), pp. 1349–1359.
- [11] A. M. BLOKHIN AND A. A. IORDANOVICH, *Numerical investigation of a gas dynamic model for charge transport in semiconductors*, COMPEL, 18 (1999), pp. 6–37.
- [12] K. BLOTEKJAER, *Transport equations for electron in two-valley semiconductors*, IEEE Trans. Electron. Devices, ED-17 (1970), pp. 38–47.
- [13] J. F. CLARKE, *Compressible Flow Produced by Distributed Sources of Mass: An Exact Solution*, Technical Report CoA Report 8710, College of Aeronautics, Cranfield Institute of Technology, Cranfield, UK, 1987.
- [14] J. F. CLARKE AND E. F. TORO, *Gas flow generated by solid-propellant burning*, in Proceedings of the International Conference on Numerical Simulation of Combustion Phenomena, INRIA, Sophia Antipolis, France, R. Glowinski, B. Larrouturou, and R. Teman, eds., Lecture Notes in Phys. 241, Springer-Verlag, New York, 1985, pp. 192–205.
- [15] E. FATEMI, J. JEROME, AND S. OSHER, *Solution of hydrodynamic device model using high-order nonoscillatory shock capturing algorithms*, IEEE Trans. Computer-Aided Design, 10 (1991), pp. 232–244.
- [16] C. L. GARDNER, J. W. JEROME, AND D. J. ROSE, *Numerical methods for the hydrodynamic device model: Subsonic flow*, IEEE Trans. Computer-Aided Design, 8 (1989), pp. 501–507.
- [17] C. L. GARDNER, *Numerical simulation of a steady-state electron shock wave in a sub-micrometer semiconductor device*, IEEE Trans. Electron. Devices, 38 (1991), pp. 392–398.
- [18] V. GRUZINSKI, E. STARIKOV, P. SHIKTOROV, L. REGGIANI, AND L. VARANI, *Linear and nonlinear analysis of microwave power generator in sub-micrometer  $n^+ - n - n^+$  InP diodes*, J. Appl. Phys., 76 (1994), pp. 5260–5271.
- [19] W. HAENSCH, *The Drift-Diffusion Equation and its Application in MOSFET Modeling*, Springer-Verlag, Wien, 1991.
- [20] A. HARTEN AND S. OSHER, *Uniformly high-order accurate nonoscillatory schemes*, SIAM J. Numer. Anal., 24 (1987), pp. 279–309.
- [21] C. D. LEVERMORE, *Moment closure hierarchies for kinetic theories*, J. Statist. Phys., 83 (1996), pp. 331–407.
- [22] C. HIRSCH, *Numerical Computation of Internal and External Flows, Vol. I*, Wiley, London, 1988.
- [23] J. W. JEROME AND C. W. SHU, *Energy models for one carrier transport in semiconductor devices*, IMA Vol. Math. Appl. 59, W. M. Coughran, Jr., J. Cole, P. Lloyd, and J. K. White, eds., Springer-Verlag, New York, 1994, pp. 185–207.
- [24] D. JOU, J. CASAS-VAZQUEZ, AND G. LEBON, *Extended Irreversible Thermodynamics*, Springer-Verlag, Berlin, 1993.
- [25] A. JUNGEL AND C. POHL, *Numerical simulation of semiconductor devices: Energy transport and quantum hydrodynamic models*, in Proceedings of the Sixth International Workshop on Computational Electronics, Osaka, Japan, IEEE, Los Alamitos, CA, 1998, pp. 230–233.
- [26] R. J. LEVEQUE, *Numerical Methods for Conservation Laws*, Birkhäuser-Verlag, Basel, 1992.
- [27] A. MARROCCO AND PH. MONTARNAL, *Simulations des modèles “energy transport” à l’aide des éléments finis mixtes*, C. R. Acad. Sci. Paris Sér. I Math., 323 (1996), pp. 535–541.
- [28] I. MÜLLER AND T. RUGGERI, *Extended Thermodynamics*, Springer Tracts in Natural Philosophy 37, Springer-Verlag, New York, 1991.
- [29] O. MUSCATO, R. M. PIDATELLA, AND M. FISCHETTI, *Monte-Carlo and hydrodynamics simulation of a one-dimensional  $n^+ - n - n^+$  silicon diode*, Electronics VLSI Design, 6 (1998), pp. 247–250.
- [30] G. STRANG, *Accurate partial difference methods. II. Non-linear problems*, Numer. Math., 6 (1964), pp. 37–46.
- [31] V. ROMANO AND G. RUSSO, *Numerical solutions for hydrodynamical models of semiconductors*,  $M^3AS$ , in press.
- [32] H. NESSYAHU AND E. TADMOR, *Non-oscillatory central differencing for hyperbolic conservation laws*, J. Comput. Phys., 87 (1990), pp. 408–463.
- [33] E. F. TORO, *Riemann Solvers and Numerical Methods for Fluid Dynamics*, Springer-Verlag, Berlin, 1997.
- [34] E. F. TORO AND S. J. BILLETT, *Centred TVD Schemes for Hyperbolic Conservation Laws*, IMA J. Numer. Anal., 20 (2000), pp. 47–79.

- [35] T. VOGELSANG AND W. HAENSCH, *A novel approach for including band structure effects in a Monte-Carlo simulation of electron transport in silicon*, J. Appl. Phys., 70 (1991), pp. 1493–1499.
- [36] B. VAN LEER, *On the relation between the upwind-differencing schemes of Godunov, Engquist-Osher and Roe*, SIAM J. Sci. Stat. Comput., 5 (1984), pp. 1–20.
- [37] A. M. ANILE AND P. PIETRA, *private communication*, 1999.